Patterns in simulated turbulent channel flow

By D. Stretch

1. Motivation and objectives

The arrival of direct numerical simulations as a practical research tool for studying the fundamental physics of turbulent flow has provided data of unprecedented detail. The volume of data available, however, presents its own difficulties and has generated a need for new methods of interrogating the available data and extracting information of physical importance.

The detailed nature of databases from numerical simulations makes them ideally suited to studying the spatial structure or topology of the flow kinematics. The identification of organized motions or coherent structures in turbulent flows is a controversial area of research. The key difficulty is the specification of appropriate criteria for the identification of these structures. In particular, the subjectivity often associated with such choices is a major drawback. One consequence of this is that different researchers, using different criteria, have "discovered" a variety of structures, and it remains unclear how they are related to one another. For example, flow visualization experiments have shown that elongated low and high speed streaks are characteristic of the flow near the wall (e.g. Kline et al, 1967), while inclined horseshoe or hairpin shaped vortices have apparently been observed in the outer flow (e.g Head & Bandyopadhyay, 1981). Similar vortices have also been observed in the near wall region (e.g. Britter & Stretch, 1985; Robinson et al, 1989). Conditional sampling analyses have shown that protruding shear layers are common features of the near wall flow, and are associated with a large contribution to turbulence production (Johansson et al, 1987). Analysis of the flow kinematics using the method of proper orthogonal decomposition, which employs a global optimization criterion, has also been carried out to yield quasi-streamwise vortices in the near wall region, with attached double-roller eddies spanning the flow (Moin & Moser, 1989).

The surface stress is a key diagnostic in wall-bounded turbulent flows. Large fluctuations in the stress are believed to be associated with intermittent "bursting" events during which a large proportion of the turbulence production takes place. If this is so, then a detailed investigation of the structure of the surface stress and its spatial relationship to events within the flow could have wide application in drag reduction and other aspects of flow control. The initial phase of this research project, therefore, concentrated on the surface stress field.

The main objectives of the research project may be summarized as follows.

(a) Carry out a statistical analysis of the instantaneous surface stress in a simulated turbulent channel flow, including comparison with multi-point experimental data from a zero pressure gradient turbulent boundary layer (Britter

and Stretch, 1985).

(b) Apply a simple pattern-recognition procedure to educe the characteristic spatial structure of various flow diagnostics. Initially attention was focused on the instantaneous streamwise component of the surface stress. The objective was to investigate the relationship between characteristics features of the surface stress and dynamically significant events occurring within the flow.

(c) As initially implemented the pattern analysis was restricted to investigating the structure of a scalar diagnostic (such as the streamwise surface stress fluctuations) in two spatial dimensions. A final objective of this program was to extend the pattern recognition analysis to examine the whole 3-D structure of the flow. One of the main questions we wished to address was "What are the spatial relationships among the many different kinematic structures that have been proposed by previous investigators?".

2. Outline of the pattern recognition methodology

The pattern recognition method used for the present study is based on work by Townsend (1979), Savill (1979) and (particularly) Mumford (1982,1983). Recent applications of this pattern analysis method have been reported by Ferre and Giralt (1989a,b). These studies were all concerned with the analysis of multipoint experimental measurements in turbulent wakes and boundary layers, and were confined to locating flow patterns in a 2-dimensional plane of data. The present study seems to be the first application of this type of approach to data from numerically simulated turbulent flow. This has allowed the full 3-D structure of the flow to be studied using an extension of the method employed by the above-mentioned authors. The low Reynolds number simulation of turbulent channel flow by Kim, Moin and Moser (1987) was the primary source of data for the present study ($Re_\theta = 287$).

In general terms the objective of the pattern recognition analysis is to educe a statistically significant spatial organization of a given flow diagnostic. For example, suppose the flow diagnostic is smoke or dye concentrations resulting from injection into the sublayer of a turbulent boundary layer. If an ensemble of photographs showing the structure of the smoke (dye) concentration field just downstream of the injection position is examined, it is clear that a streaky pattern would be recognized as the most probable spatial organization of that flow diagnostic. Note that in order to recognize this, a translational invariant pattern recognition method is required, since the streaks may be at different spanwise locations at the instant of each photograph.

Details of the pattern recognition strategy may be outlined as follows. Consider a field of data $D(\mathbf{x})$, which for present purposes is assumed to be a scalar function of a position vector $\mathbf{x} \in \mathbf{R}^3$.

$$D(\mathbf{x}) = \{d(i,j,k),\ 0 \le i \le n_1,\ 0 \le j \le n_2,\ 0 \le k \le n_3\}$$

In the present context D is some chosen diagnostic of the turbulent field. Note that the pattern analysis procedure can easily be generalized to include time evolution and vector functioned diagnostics. We now define a pattern field $P(\hat{\mathbf{x}})$, a scalar function of the position vector $\hat{\mathbf{x}} \in \mathbf{R}^3$.

$$P(\hat{\mathbf{x}}) = \{p(i,j,k),\ 0 \leq i \leq m_1,\ 0 \leq j \leq m_2,\ 0 \leq k \leq m_3\}$$

where $m_1,\ m_2,\ m_3 \leq n_1,\ n_2,\ n_3$.

The first step in the pattern analysis is to initialize the pattern field $P(\hat{\mathbf{x}}) = P_0(\hat{\mathbf{x}})$. Next a convolution is performed between the pattern and the data fields.

$$C(\mathbf{x}) = P(\hat{\mathbf{x}}) * D(\mathbf{x})$$

Patterns which have a shape similar to the input pattern P are then located in the data field D by searching for all the local maxima in the convolution function C. Note that there is no threshold criterion used in the pattern selection (although it is, of course, simple to include one if desired). Once the patterns have been located in the data they are extracted and ensemble averaged to yield an updated estimate of P, and the process is repeated. The iterative procedure results in a pattern P which on average has the best correlation with the instantaneous patterns located in the data field D.

Note that the pattern recognition method does not employ an absolute criterion for locating patterns. The pattern selection depends on a relative criterion, namely that locally the flow kinematics are more similar to the reference pattern P than elsewhere in that neighbourhood, where the measure of similarity is the magnitude of the convolution (or cross-correlation) between the reference pattern and the data. The use of convolution for pattern recognition is a well established and tested method (see e.g. Duda and Hart, 1973)

The pattern analysis procedure outlined above has translational invariance but not scale or rotational invariance; it is assumed that the patterns can occur at any position $\mathbf{x}$ in the data, but the orientation and size of the patterns is always assumed to be the same. It is possible to include scale and rotational invariance in pattern recognition schemes such as this one, but it involves considerable complication of the analysis, and thus has not been implemented to date.

It shall be shown later (by examples) that the results of the pattern search do not appear to be sensitive to the choice of initial pattern P_0. In the present investigation P_0 was usually specified so that the first iteration simply performed a spatial averaging operation in one plane of the 3-D data field.

The results of the pattern analysis may be assessed in a variety of objective tests. For example, the statistical significance of the ensemble averaged patterns P may be tested using standard methods from sampling theory. The proportion of the data volume occupied by the patterns and the similarity between the ensemble averaged pattern P and the instantaneous flow field is information available directly from the pattern recognition algorithm.

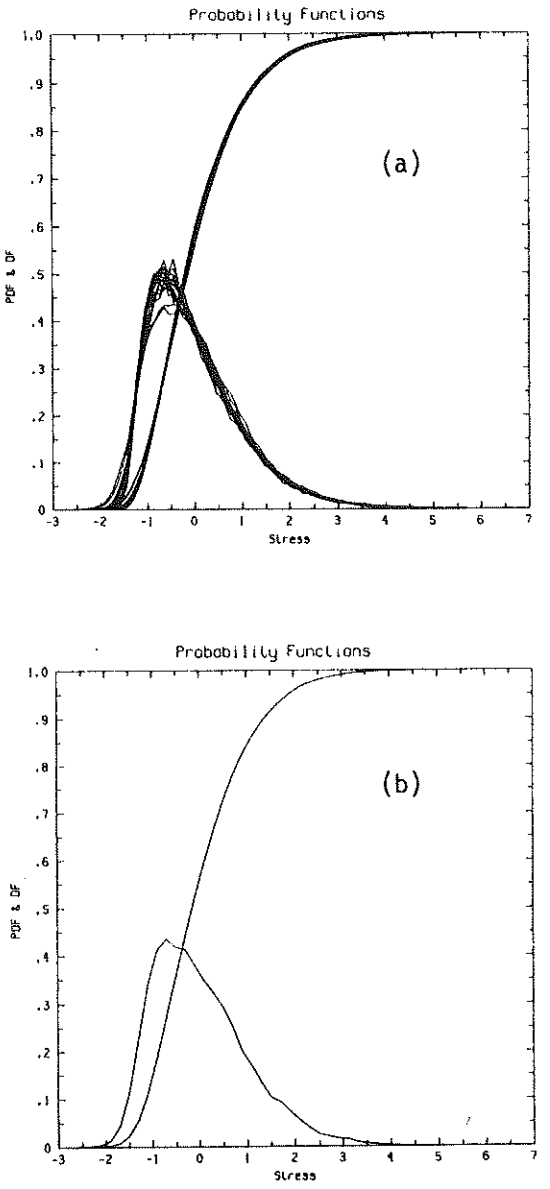

FIGURE 1. Probability density and distribution functions for the streamwise surface stress fluctuations : (a) experimental data $915 \leq Re_\theta \leq 2140$, (b) simulation data $Re_\theta = 287$. The stress fluctuations are normalized by their rms values.

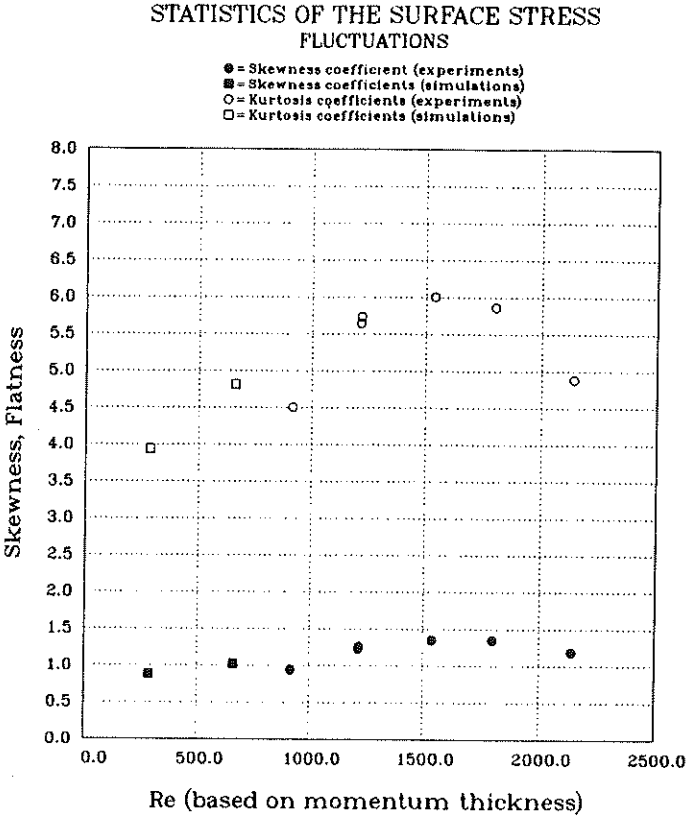

FIGURE 2. Skewness and kurtosis coefficients of the streamwise surface stress fluctuations from experiments and simulations.

3. Summary of results

3.1 One-point statistics

The basic 1-point statistics for the streamwise surface stress fluctuations from both the simulations and experiments are shown in figures 1 and 2. The probability density functions of the stress fluctuations are positively skewed and have a kurtosis somewhat higher than a Gaussian distribution. Values for the skewness and kurtosis coefficients $S = \overline{\tau^3}/\tau'^3$, $F = \overline{\tau^4}/\tau'^4$ from the experimental measurements are in the range $1.0 \leq S \leq 1.6$ and $4.0 \leq F \leq 6.0$, which may be compared with the Gaussian values $S = 0$ and $F = 3$. The experimental data show a slight increase with Reynolds number. The simulation results of $S = 0.88$, $F = 3.9$ at a low Reynolds number $Re_\theta \simeq 287$ are consistent with this trend. Preliminary simulation results at $Re_\theta \simeq 660$ (also shown in fig 1) are $S = 1.06$ and $F = 5.04$, which is also consistent with the experiments. The skewness in the surface stress is apparently caused by the way the low and high stress regions

are generated. High surface stresses are associated with the "sweep" (or fourth quadrant, Q4) event during which high-speed fluid moves toward the wall. Low stresses are associated with the "burst" (or second quadrant, Q2) event during which low speed fluid moves away from the wall. The low speed fluid involved in the burst must be drawn from regions near the wall and at the sides of the event, a motion which is apposed by the strong viscous stresses in the sub-layer.

The ratio of the root mean square streamwise stress fluctuations to the mean wall stress was experimentally determined to be $\tau'/\overline{\tau} = 0.4 \pm 0.1$, increasing slightly with Reynolds number. The simulation results are 0.36 and 0.39 at $Re_\theta = 287, 660$ respectively, again in reasonable agreement with the experiments.

From the probability density function, it can be seen that the instantaneous streamwise surface stress is less than the mean value for 55 – 60% of the time (increasing with Reynolds number). The most probable value is approximately $0.5\tau'$ below the mean. The pdf drops off sharply at $2.0\tau'$ below the mean. Note that since $\tau'/\overline{\tau} \simeq 0.4$, stress fluctuations exceeding $2.5\tau'$ below the mean would imply reversed flow adjacent to the wall. From the pdf's it appears that the instantaneous (near) surface streamlines are topologically free of critical points, or at least that their occurrence is extremely rare.

3.2 Two-point statistics

Two-point correlation functions for streamwise and transverse separations are shown in figure 3. The experimental data and simulation results are shown with separations scaled on wall variables ν and $u_\star$. A streamwise advection velocity of $10u_\star$ for the stress fluctuations was measured experimentally using two-point measurements with streamwise separations. This value is consistent with those obtained from previous analyses of the simulation data bases (Alfredsson et al (1988), Johansson et al (1987), Guezennec et al (1987), Hussain et al (1987), Swearingen et al 1987). If this advection velocity is used to convert the time series experimental measurements to a spatial analog there is surprisingly good agreement with the simulation results. Conclusions regarding the scaling of the two-point correlations on wall variables should, however, be made with care, since the range of Reynolds number covered by the data is limited.

The two-point correlations for spanwise separations do not scale as well as those for streamwise separations; there is a decrease in the magnitude of the negative loop for $\triangle z^+ \geq 40$ with increasing Reynolds number. This trend has been tentatively confirmed by the preliminary channel simulations at $Re_\theta \simeq 660$ and by the boundary layer simulations of Spalart (1988). The reason for this effect is not clear, but it probably reflects the broader range of scales in the higher Reynolds number cases.

3.3 Results of 2-D pattern analyses

The application of the pattern analysis to the simulation data was begun using 2-D data comprising the streamwise component of the fluctuating surface

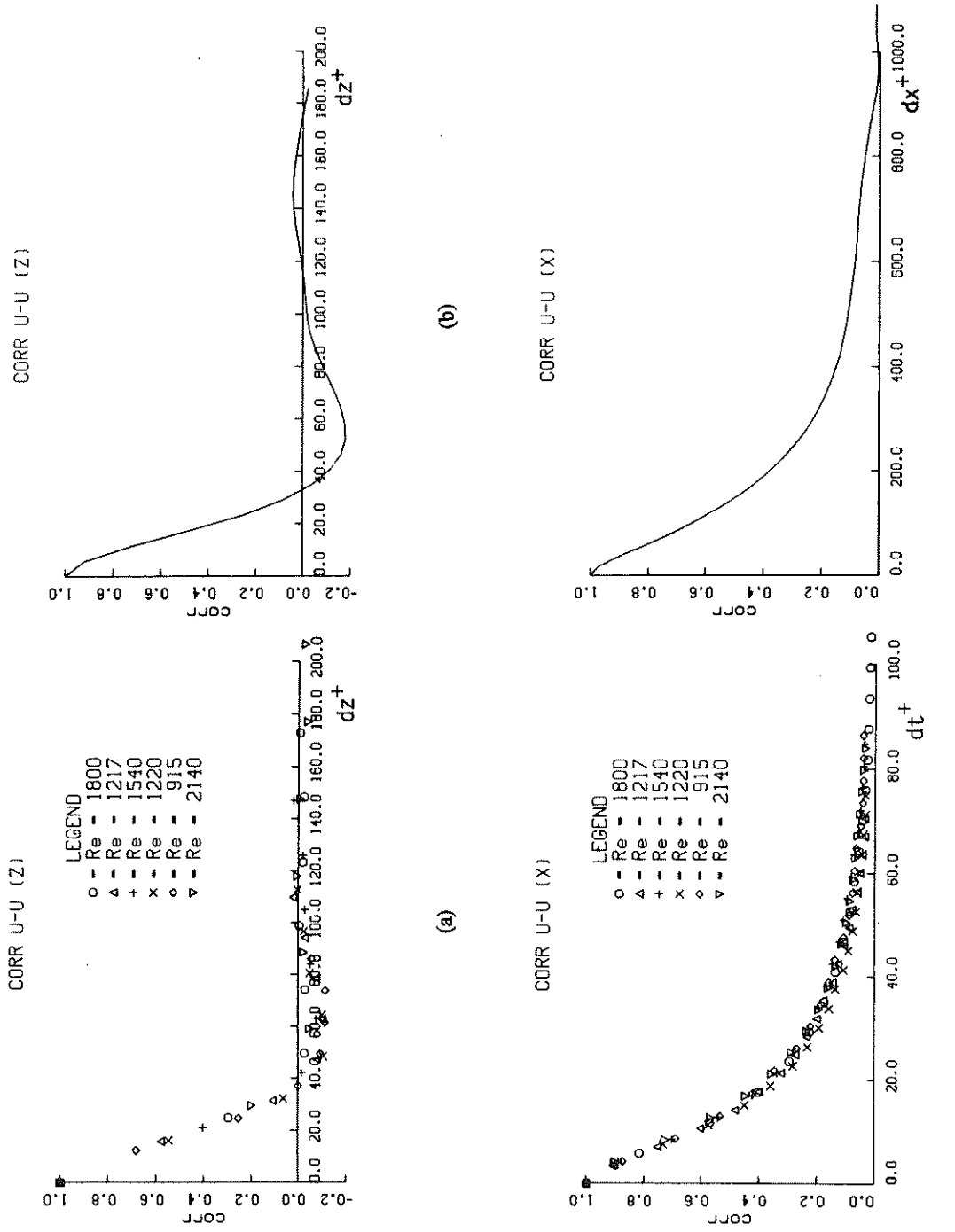

FIGURE 3. Two point correlation functions of the streamwise surface stress fluctuations : (a) experiments, (b) simulations.

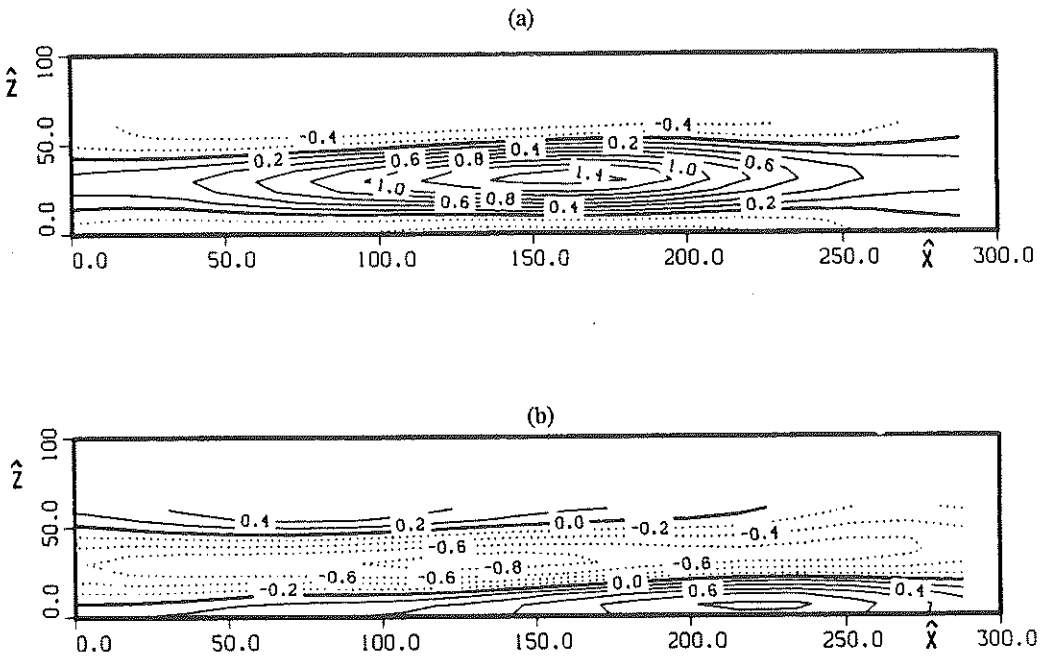

FIGURE 4. Results from a 2-D pattern analysis of the streamwise surface stress fluctuations : (a) high stress regions, (b) low stress regions. The stress fluctuations are normalized their rms values. Dotted lines are used for negative values.

stress at the wall. Several data fields consisting of 128×128 values of the stress, spaced as $\triangle x^+ = 18.0$, $\triangle z^+ = 6.0$, were used for the analyses. The results were compared with those from similar analyses of multi-point experimental measurements.

Using a simple spatial filter as the initial pattern for the iterative pattern analysis, the structure of locally high and low stress regions were investigated. For example, initial patterns defined by

$$p_0(i,j,k) = \begin{cases} \pm 1, & \text{if } 7 \leq i \leq 11,\ j = 1,\ 3 \leq k \leq 9; \\ 0, & \text{otherwise.} \end{cases}$$

where the pattern size was $m_1 = 17$, $m_2 = 1$, $m_3 = 11$, were used to obtain the results shown in figure 4. Five iterations were performed to obtain this result, although there was little variation after the second iteration.

The high- and low-stress patches have some distinct characteristics. High stress regions have a larger amplitude and are somewhat more localized in space than the low stress regions. Non-dimensionalized with the inner variables ν and u_τ, the amplitudes and scales of these stress patterns have been found to be broadly consistent with those educed from experimental data.

3.4 Results of 3-D pattern analyses

The data used for the 3-D pattern analysis comprised fields of $128 \times 128 \times 16$ values in the x, z, and y directions respectively, spaced as $\triangle x^+ = 18.0$, $\triangle z^+ = 6.0$ and $\triangle y^+ \simeq 10.0 \pm 0.1$.

Pattern analyses for a range of different flow diagnostics and initial patterns P_0 have been performed. The examples described below illustrate some of the main results. Note that all references to lengths or positions are non-dimensionalized using the length scale $\nu/u_\star$. Velocities are non-dimensionalized with $u_\star$, and vorticity by the scale $u_\star/\delta$, where δ is the channel half-width (dividing by 180 gives values of the vorticity scaled by ${u_\star}^2/\nu$). Furthermore, co-ordinates x, y and z refer to the data space D, while $\hat{x}$, $\hat{y}$ and $\hat{z}$ refer to the pattern space P.

Example 1 : Diagnostic = streamwise velocity fluctuations.

In this example, a simple initial pattern P_0, which was designed to select near-wall shear layers in the first iteration, was used. That is

$$p_0(i,j,k) = \begin{cases} +1, & \text{if } 10 \le i \le 15,\ j = 2,\ 3 \le k \le 13; \\ -1, & \text{if } 17 \le i \le 22,\ j = 2,\ 3 \le k \le 13; \\ 0, & \text{otherwise.} \end{cases}$$

where the pattern size was $m_1 = 31$, $m_2 = 15$, $m_3 = 15$. Note that the indices i, j, and k refer here to the streamwise ($\hat{x}$), normal ($\hat{y}$), and spanwise ($\hat{z}$) directions respectively. Only horizontal translations were allowed in this pattern search.

The results of the pattern eduction are shown in figure 5. After 4 iterations, the educed pattern is seen to comprise asymmetric high and low speed regions in the xz plane at $\hat{y}^+ = 10$. Note the occurrence of smaller scale high and low peaks within the elongated "streaks". These high/low pairs seem to occur alongside one another separated by $\triangle \hat{z}^+ \simeq 50$. An xy cross-section through the pattern at $\hat{z}^+ = 42$ is also shown in figure 5. An elevated shear layer typical of those obtained by conditional sampling methods can be seen.

Ensemble averages of flow diagnostics other than the streamwise velocity fluctuations were examined in the regions centered around the located patterns. The streamwise vorticity is shown in the yz plane at $\hat{x}^+ = 270$ (figure 5c), and in the xy plane at $\hat{z}^+ = 42$ (figure 5d). It can be seen that a single dominant positive streamwise vortex is associated with the near-wall high/low peaks in the u field.

In this example, 57 patterns were identified in a single data field D. The average value of the normalized cross-correlation coefficient between the final ensemble averaged pattern and the 57 instantaneous patterns was 0.36. The data used to obtain the ensemble average comprised 82% of the whole $128 \times 128 \times 16$ data field. These figures are typical of all the cases described here.

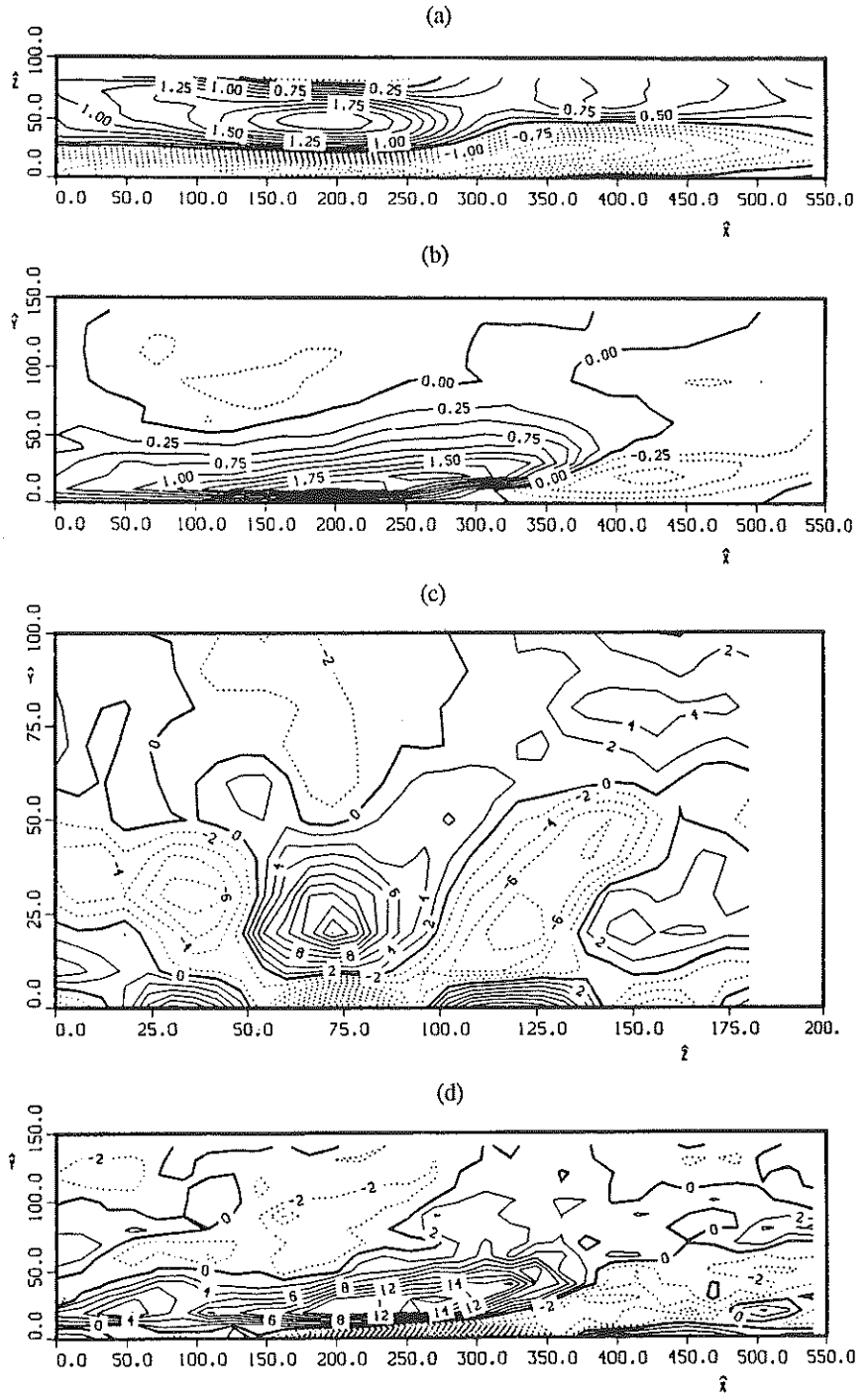

FIGURE 5. Results from example 1 of the 3-D pattern analysis: (a) u field in xz plane at $\hat{y}^+ = 10$, (b) u field in xy plane at $\hat{z}^+ = 42$, (c) ω_x field in zy plane at $\hat{x}^+ = 270$, (d) ω_x field in xy plane at $\hat{z}^+ = 50$. Velocity fluctuations are normalized by $u_\star$ and vorticity fluctuations by $u_\star/\delta$. Dotted lines are used for negative values.

Example 2 : Diagnostic = streamwise vorticity (near wall).

In this example the initial pattern field P_0 was chosen to perform a simple spatial averaging in the yz plane. That is

$$p_0(i,j,k) = \begin{cases} +1, & \text{if } i = 8,\ 2 \leq j \leq 4,\ 2 \leq k \leq 8; \\ 0, & \text{otherwise.} \end{cases}$$

where the pattern size was $m_1 = 15$, $m_2 = 5$, $m_3 = 9$. Vertical translations were allowed in the pattern search, but were constrained so that the center of the pattern was in the region $20 \leq y^+ \leq 60$. The objective was to locate and examine quasi-streamwise vortices in the near-wall region of the flow.

Results of the pattern eduction are shown in figure 6. The pattern comprises a vortex inclined at a small angle to the horizontal axis, roughly 15 degrees. There is only weak evidence of spanwise pairing of opposite signed vortices. However, there is strong negative vorticity underneath and downstream of the primary positive vortex. Near the wall this arises to satisfy the no-slip boundary condition. Note, however, that the region of negative vorticity is also inclined to the wall and appears to separate from the wall sufficiently far downstream. This is further illustrated in example 3 below.

The ensemble averaged streamwise and vertical velocity fluctuations associated with the patterns are also shown in figures 6c and 6d. The streamwise velocity field has the same features as were found in example 1. The vertical velocity field shows the expected upwelling over the low speed "streak" and flow towards the wall over the high speed region.

Example 3 : Diagnostic = streamwise vorticity (outer flow).

In this example, the initial pattern field P_0 was identical to the previous example, except that vertical translations in the pattern search were constrained to the region $80 \leq y^+ \leq 130$ in order to examine the structure of the streamwise vorticity in the outer part of the flow.

Results of the pattern eduction are shown in figure 7. As in example 2, the pattern comprises inclined vortices. The scale of the vortices seems to have increased, as has the inclination angle. Once again we note how the primary pairing of opposite sign vortices is in the vertical and streamwise directions, but not in the spanwise direction.

Example 4 : Diagnostic = spanwise velocity fluctuations.

A simple attached eddy of the type proposed by Townsend (1976) may be expected to give rise to transverse velocity fluctuations of the same sign in elongated regions extending from the wall to the outer flow. Preliminary study of the instantaneous velocity fields from the simulations suggested that such features were indeed present. This motivated a pattern analysis using the w velocity field as the flow diagnostic. The initial pattern was designed to select (after spatial

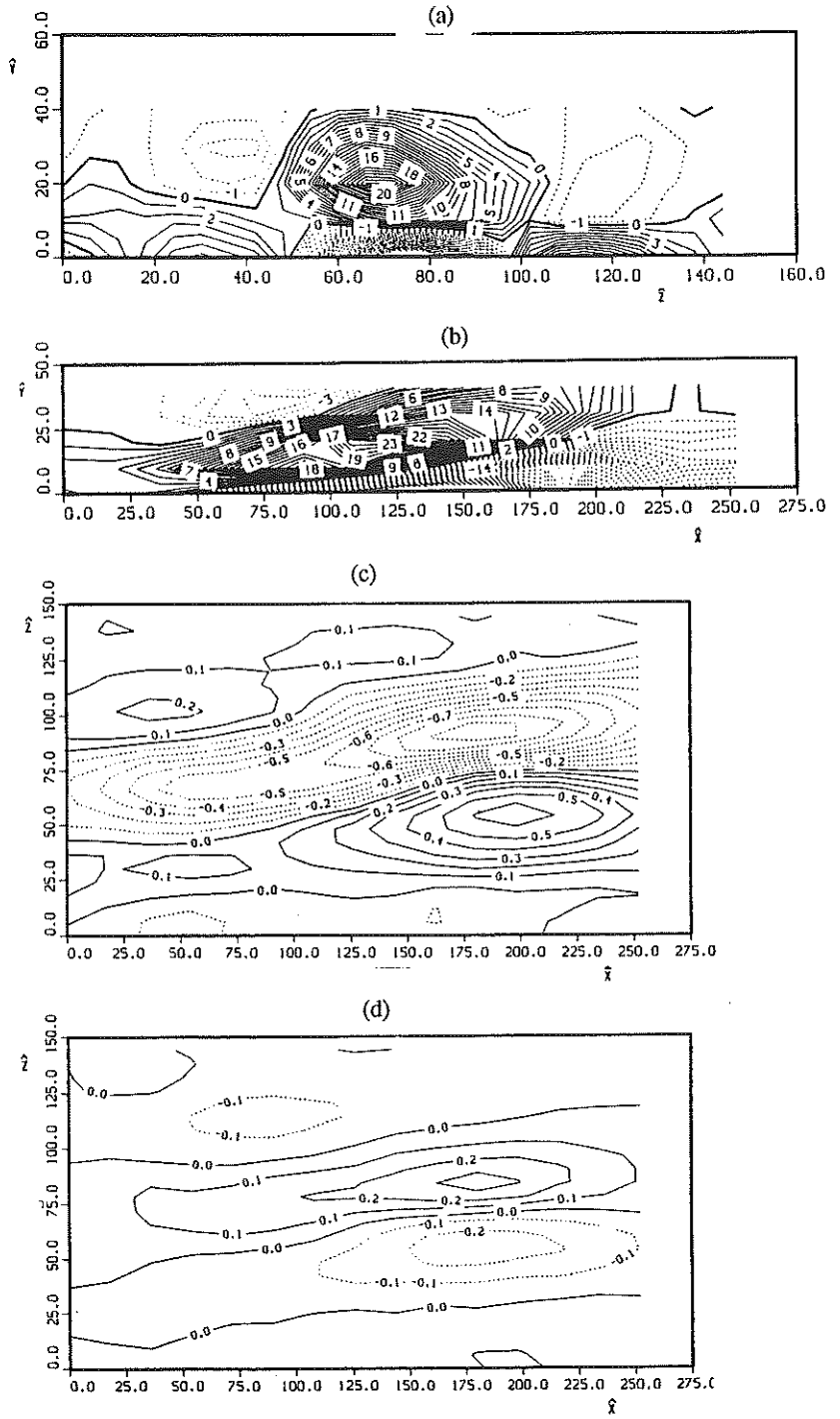

FIGURE 6. Results from example 2 of the 3-D pattern analysis: (a) ω_x field in xy plane at $\hat{x}^+ = 126$, (b) ω_x field in xy plane at $\hat{z}^+ = 72$, (c) u field in xz plane at $\hat{y}^+ = 0$, (d) v field in xz plane at $\hat{y}^+ = 0$. Normalization of the data as for figure 5.

smoothing) regions of locally high transverse velocity in the outer part of the flow ($y^+ \simeq 100$). That is

$$p_0(i,j,k) = \begin{cases} +1, & \text{if } 3 \leq i \leq 7,\ 10 \leq j \leq 12,\ 5 \leq k \leq 11; \\ 0, & \text{otherwise.} \end{cases}$$

where the pattern size was $m_1 = 9$, $m_2 = 15$, $m_3 = 15$. Only horizontal translations were allowed in the pattern search.

A result from this pattern analysis is shown in figure 8a. The educed pattern for the w field comprises elongated positive and negative (paired) regions extending from the wall to the outer part of the flow (the channel half width is at $y^+ = 180$). Examination of other flow diagnostics has shown how these paired w fluctuations are linked to the shear layers near the wall. In figure 8b, data of the instantaneous w field in an xy plane is shown as an example of an occurrence of the educed w pattern.

Summary

The main contribution of the pattern analysis has been to clarify the spatial relationships among various flow structures. In particular, we have used the method to investigate the relationships among between near-wall high/low speed streaks, near-wall shear layers, and quasi-streamwise vortices (or vortex pairs). These structures have been observed or educed from flow visualization and/or conditional sampling analyses by many previous investigators, so their presence in the patterns obtained in the present investigation is neither new nor surprising. However, the unification of all these observations seems to be a particular achievement of the present analysis. A summary of the main conclusions is presented schematically in figure 9.

4. Future plans

The major objectives of this research project as outlined in section 1 above have been achieved. In particular, a pattern recognition procedure for analysing scalar fields in two or three spatial dimensions has been successfully implemented and used to study the structure of simulated turbulent channel flow. The full results of this work are currently being written up for publication.

There are several ways in which the present research project may evolve, and the following are some in progress and planned for the immediate future.

4.1 Pattern analysis

Application to additional flow diagnostics

To date the pattern analysis has been limited to the study of the streamwise and spanwise velocity fluctuations and the streamwise vorticity, although the structure of other flow diagnostics at the pattern locations have also been examined. There are obvious extensions of the work in applying the pattern

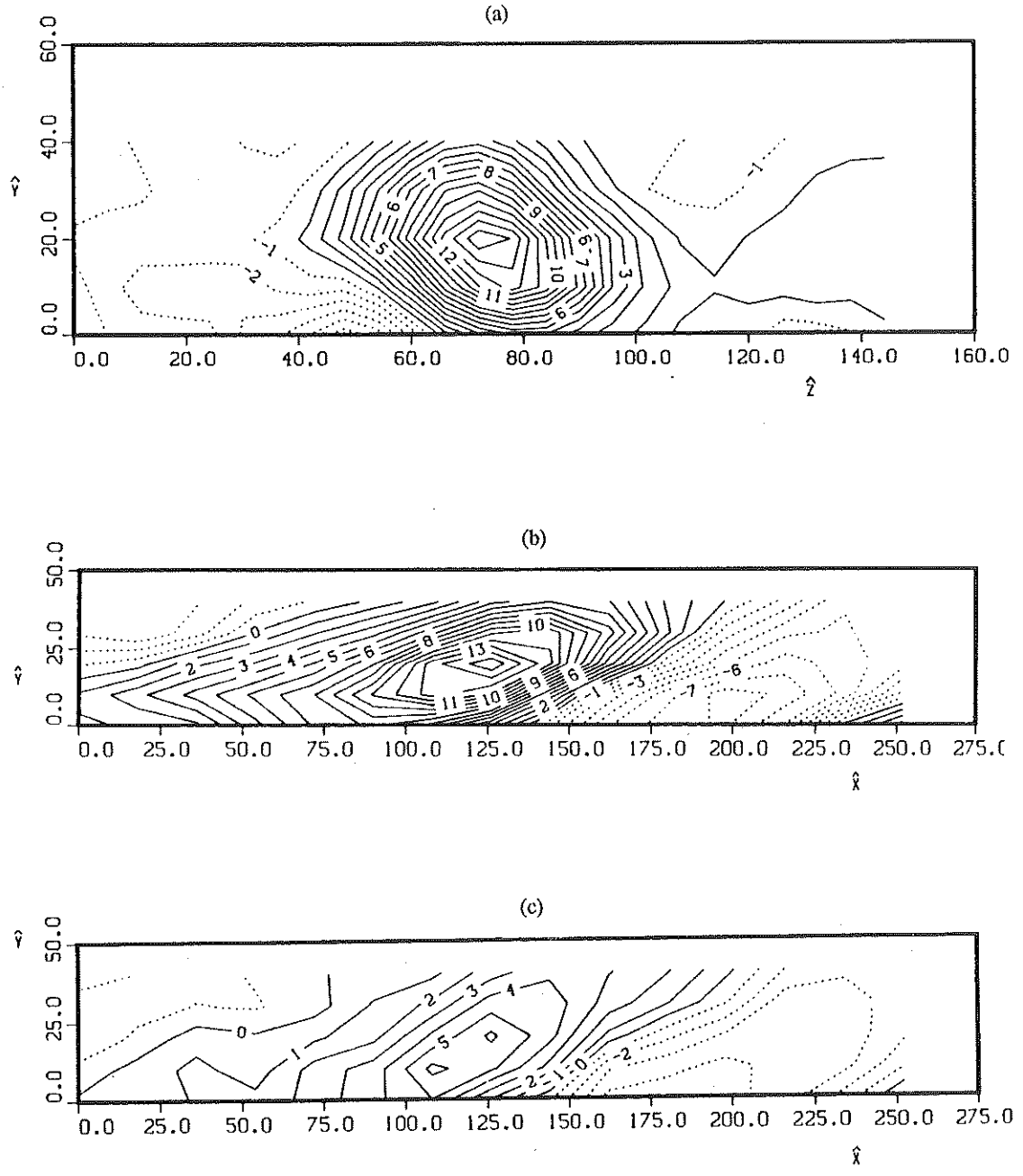

FIGURE 7. Results from example 3 of the pattern analysis: (a) ω_x field in xy plane at $\hat{x}^+ = 126$, (b) ω_x field in xy plane at $\hat{z}^+ = 72$, (c) ω_y field in xy plane at $\hat{z}^+ = 72$. Normalization of the data as for figure 5.

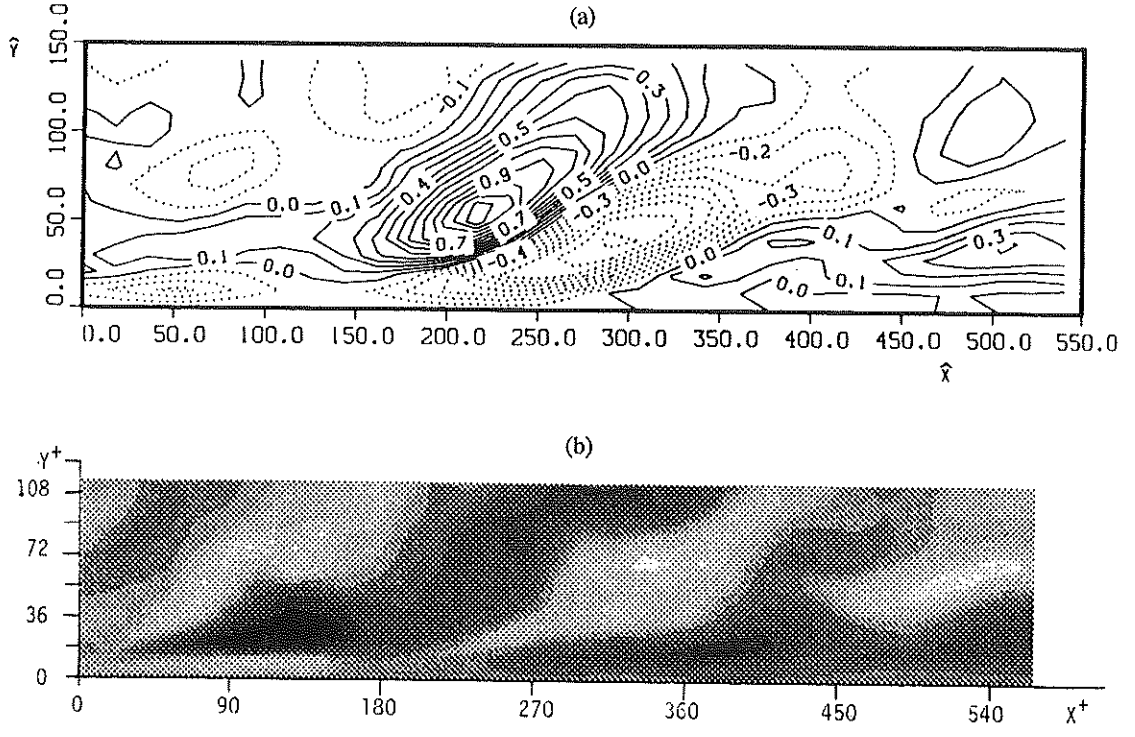

FIGURE 8. Results from example 4 of the pattern analysis: (a) w field in xy plane at pattern center, (b) example of an instantaneous w field in an xy plane. The w velocity fluctuations are normalized with u_*, and dotted lines are used for negative values in (a), and shades of gray are used in (b).

recognition to further diagnostics of the flow directly. Examples which have not yet been analysed are the instantaneous Reynolds stresses, vertical velocity fluctuations, and components other than streamwise of the vorticity field. In addition, the structure of the helicity density and the local dissipation rates may also be investigated. The pattern recognition approach is particularly useful in cases where the spatial shapes of features and/or their spatial relationships are required.

An analysis presently in progress is to use the product of the pressure and the vorticity as a diagnostic intended for detecting vortices (as distinct from simply vorticity). Vortices which display roughly circular streamlines in a plane perpendicular to their axes characteristically have low pressure regions in their cores (Robinson et al, 1989). Alternatively, the pattern analysis procedure may be used to examine the spatial structure of the eddy, streaming, and convergence zones defined by Hunt et al, 1988.

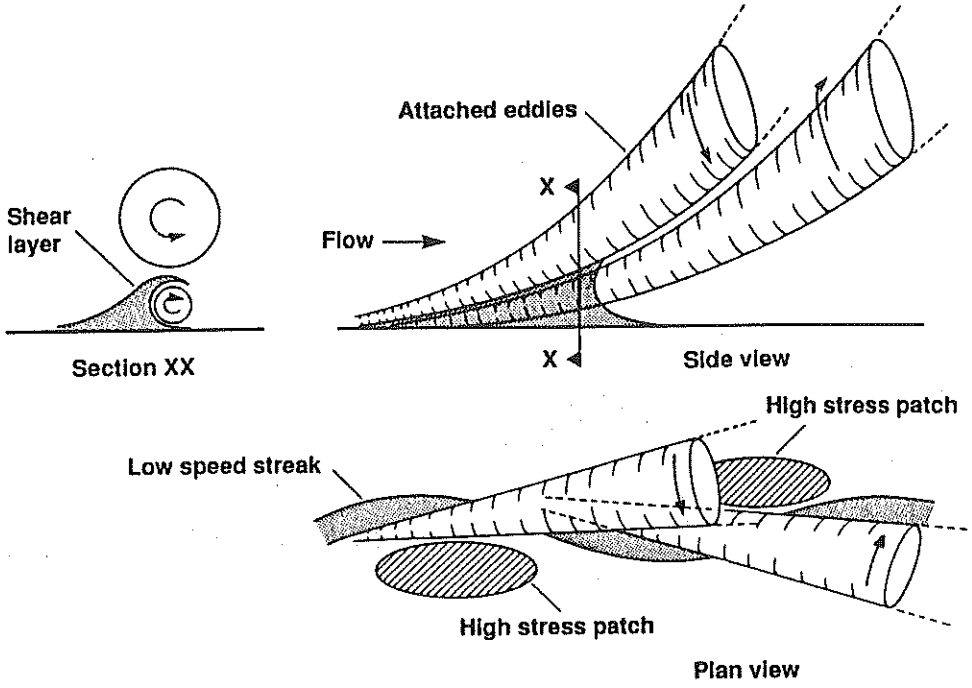

FIGURE 9. Sketch giving a simplified summary of the pattern analysis results.

Application to simulated boundary layer data

An interesting extension of the present research would be the application of the pattern analysis to the simulated boundary-layer data of Spalart (1988). While it is expected that the near-wall structure of the boundary-layer and channel flows is at least qualitatively similar, significant differences may be present in the outer flow structure. Application of the pattern analysis to investigating these differences is straightforward. The boundary-layer data also covers a wider range of Reynolds number than the currently available channel flow data, with $225 \leq Re_\theta \leq 1410$. This may enable Reynolds number effects to be assessed, at least within the limited parameter range available. Application of the pattern analysis to the higher Reynolds number channel flow data, when they are available, is also planned.

4.2 Dynamics of the turbulence structures

While the pattern recognition analysis has proven to be useful for extracting information on the kinematics of the turbulence, it is limited in its ability to

provide dynamical information. It is possible to study temporal evolution using the pattern analysis, but the volume of data required increases dramatically and the details of the dynamics may in any event be unacceptably smeared by the ensemble averaging process. Furthermore, the absence of scale and rotational invariance in the pattern analysis scheme (as it is currently implemented) may also be a drawback in that context. For example, it is expected that changes in scale are an important aspect of the evolution of the vortex structures.

A more promising approach for studying the dynamics of the flow may be the analysis of simplified initial value problems. Research based on the use of linearized Rapid Distortion Theory to study the evolution of localized 3-D disturbances in a strong shear (with and without the presence of a boundary) is planned for continuing work. Previous work at CTR by Lee & Hunt (1988) and Lee, Kim & Moin (1989) has shown how prolonged straining of initially isotropic turbulence by strong shear gives rise to a "streaky" structure in the flow (a 1-component, 3-D flow in the limit of rapid and large strains). The scaling of the resulting structure, however, is unclear from the above-mentioned work. There were two length scales in the problem considered: L_0, the initial characteristic length scale of the turbulence, and $(\nu/S)^{\frac{1}{2}}$, a length scale based on the viscosity ν and the shear rate S. This issue may be analytically resolvable and efforts are underway. Furthermore, it may be worth noting that work by Jang, Benney & Gran (1986), and developments thereof currently in progress at CTR (by J. Kim), have suggested that a "direct resonance" mechanism may explain the observed scaling of the near wall streaks and the origin of associated quasi-streamwise vortices. These "resonant" modes, which have algebraic growth rates, also appear to be present in uniform shear flow. An interesting question, therefore, arises concerning the effect of curvature in the mean velocity profile on these modes. Curvature gives rise to a class of solutions comprising propogating, wave-like disturbances in the flow, as distinct from the purely convected disturbances in the absence of curvature.

Flow visualization experiments (Britter & Stretch, 1985) have suggested that a wake-like "instability" or roll-up of vertical (and transverse) vorticity associated with the low and high speed streaks may be involved in the generation of quasi-streamwise vortices near the wall. A similar mechanism has been proposed and studied by Swearingen and Blackwelder (1987). An investigation of this proposal using linearized initial value problems is planned.

4.3 Channel flow manipulation using buoyancy effects

Previous experiments by the author (Stretch, 1985 ; Britter & Stretch, 1985) have suggested that a weak stable stratification can have a profound effect on the structure of turbulent boundary layers. In particular, rapid and dramatic decreases in turbulence mass and momentum transport can occur with increasing stable stratification to the extent that it seems possible to partially laminarize the flow. These experimental observations (involving both flow visualization

and quantitative measurements) suggest that the stratification effects are closely focused on the fundamentally important dynamics of the flow. In addition to obvious applications in flow control, it thus appears that the use of stratification as a manipulative tool may be a revealing way to study the dynamics of the turbulence. It is planned to perform simulations of a stably stratified turbulent channel flow in order to study these effects.

Acknowledgements

The author is indebted to John Mumford of Cambridge University for explaining his pattern recognition strategy. Josep Ferre from the University of Barcelona also assisted with some initial analysis of the experimental data. It is a pleasure to acknowledge the contributions of Rex Britter from Cambridge University, who visited CTR this summer to collaborate with me on some of the work outlined here. I am grateful to John Kim of CTR for providing simulation data and for helpful comments on the work. Finally, I would like to acknowledge the support of the Center for Turbulence Research.

REFERENCES

ALFREDSSON, P. H., JOHANSSON, A. V., & KIM, J. 1988 Turbulence production near walls: the role of flow structures with spanwise asymmetry. Report CTR-S88, Proceedings of the 1988 Summer Program, Center for Turbulence Research.

BRITTER, R. E. & STRETCH, D. D. 1985 On the structure of turbulent boundary layers. Report for TOPEXPRESS Ltd., Cambridge, UK, June 1985.

BRITTER, R. E. & STRETCH, D. D. 1985 Flow visualization of a stably stratified boundary layer. IUTAM Symp. on Mixing in Stratified Fluids, Margaret River, Western Australia, 25-28 Aug., 1985.

DUDA, R. O. & HART, P. E. 1973 *Pattern Classification and Scene Analysis.* J. Wiley & Sons.

FERRE, J. A. & GIRALT, F. 1989a Pattern-recognition analysis of the velocity field in plane turbulent wakes. *J. Fluid Mech.* **198**, 27-64.

GUEZENNEC, Y. G., PIOMELLI, U., & KIM, J. 1987 Conditionally-averaged structures in wall-bounded turbulent flows. Report CTR-S87, Proceedings of the 1987 Summer Program, Center for Turbulence Research.

HEAD, M. R. & BANDYOPADHYAY, P. 1981 New aspects of turbulent boundary-layer structure. *J. Fluid Mech.* **107**, 297-338.

HUNT, J. C. R., WRAY, A. A., & MOIN, P. 1988 Eddies, streams, and convergence zones in turbulent flows. Report CTR-S88, Proceedings of the Summer Program, Center for Turbulence Research.

HUSSAIN, A. K. M. F., JEONG, J., & KIM, J. 1987 Structure of turbulent shear flows. Report CTR-S87, Proceedings of the 1987 Summer Program, Center for Turbulence Research.

JANG P. S., BENNEY, D. J., & GRAN, R. L. 1986 On the origin of streamwise vortices in a turbulent boundary layer. *J. Fluid Mech.* **169**, 109-123.

JOHANSSON, A. V., ALFREDSSON, P. H., & KIM, J. 1987 Shear-layer structures in near-wall turbulence. Report CTR-S87, Proceedings of the 1987 Summer Program, Center for Turbulence Research.

KIM, J., MOIN, P., & MOSER, R. 1987 Turbulence statistics in fully developed channel flow at low Reynolds number. *J. Fluid Mech.* **177**, 133-166.

LEE, M. J. & HUNT, J. C. R. 1988 The structure of sheared turbulence near a plane boundary. Report CTR-S88, Proceedings of the Summer Program, Center for Turbulence Research.

LEE, M. J., KIM, J., & MOIN, P. 1989 Structure of turbulence at high shear rate. Unpublished manuscript.

MOIN, P. & MOSER, R. D. 1989 Characteristic-eddy decomposition of turbulence in a channel. *J. Fluid Mech.* **200**, 471-509.

MUMFORD, J. C. 1982 The structure of large eddies in fully developed turbulent shear flows. Part 2. The plane wake. *J. Fluid Mech.* **137**, 447-456.

ROBINSON, S. K., KLINE, S. J., & SPALART, P. R. 1989 A Review of Quasi-Coherent Structures in a Numerically Simulated Boundary Layer. NASA TM-102191.

SAVILL, A. M. 1979 Effects on turbulence of curved or distorting mean flow. Ph.D. thesis, University of Cambridge.

SPALART, P. R. 1988 Direct numerical simulation of a turbulent boundary layer up to $R_\theta = 1410$. *J. Fluid Mech.*. **187**, 61-98.

STRETCH, D. D. 1986 The dispersion of slightly dense contaminants in a turbulent boundary layers. Ph.D. thesis, University of Cambridge.

SWEARINGEN, J. D., BLACKWELDER, R. F., & SPALART, P. S. 1987 Inflectional instabilities in the wall region of bounded turbulent shear flows. Report CTR-S87, Proceedings of the 1987 Summer Program, Center for Turbulence Research.

TOWNSEND, A. A. 1976 *The Structure of Turbulent Shear Flows.* C. U. P.

TOWNSEND, A. A. 1979 Flow patterns of large eddies in a wake and in a boundary layers.. *J. Fluid Mech.* **95** 3, 515-537.